Pergamon

Int. J. Heat Mass Transfer. Vol. 39, No. 2, pp. 355–371, 1996

0017-9310/96 $9.50 + 0.00

0017-9310(95)00126-3

Surface transient temperature inversion for hidden corrosion characterisation: theory and applications

V. VAVILOV
Tomsk Polytechnic University, Russia, 634028, Tomsk, Savinykh, 3

E. GRINZATO, P. G. BISON† and S. MARINETTI
CNR-ITEF, Corso Stati Uniti, 4, 35127-Padova, Italy

and

M. J. BALES
Bales Scientific Inc., 1620 Tice Valley Boulevard, Walnut Creek, CA 94595, U.S.A.

(*Received* 6 *September* 1994 *and in final form* 24 *February* 1995)

Abstract—Corrosion in metals is simulated with variations in plate thickness which are laterally infinite in a 1D model and are represented by milled flat-bottom holes in a 2D model. Temperature contrast over corroded areas is chosen as an informative parameter, quite independent of absorbed thermal energy in the infra-red thermographic test. It is shown that, due to lower sensitivity to rear-side effects at the beginning of the thermal process and increasing 3D heat diffusion effects at the end of the process, there is an optimum time to detect corrosion. A robust inversion function is proposed and its stability against variations in tested material, heat pulse duration and observation time is analysed using numerical modelling. Corrosion in a steel specimen of 1.3 mm thickness is experimentally studied, having proved the validity of the inversion algorithm with an average accuracy of 17% for material loss ranging from 74 to 14%.

1. INTRODUCTION

The importance of reliable, fast, noncontact, non-destructive testing (NDT) of corrosion in metals becomes increasingly evident nowadays with ageing exploited aircraft, hardening safety requirements for pipelines with hazardous liquids, etc. [1]. The eddy-current and acoustic NDT methods remain the most usable technique due to their high sensitivity and safe handling. Nevertheless, its use encounters difficulties hard to overcome when the surface to be tested becomes extremely large and inspection time is limited. Non-contact laser acoustic is still an exotic and expensive technique. The interest to infra-red (IR) thermography, which has been high in recent years, has acquired new impetus with the appearance of high-speed, sensitive IR imagers working with closed-loop cooling devices. Besides this, recent achievements in image processing, including elements of artificial intelligence, allow one to expect that some inconvenient features of IR thermography, such as the presence of multiple noise, could be successfully overcome.

It is known that IR thermographic NDT has been successfully applied to non-metals and composite-materials [2, 3] where temperature signals are not dissipating for a long time period. With the appearance of a new generation of IR imagers, powerful flash tubes and computerised systems for recording and fast processing of IR images, thermal NDT moved toward milli-Kelvin (mK) signals and millisecond (ms) times, although the number of related research is not too large. A quantitative approach to evaluate IR images in terms of materials corrosion loss was reported in the inspection of aircraft panels [4]. Recently, important improvements in suppressing surface noise have been obtained by using dual-band IR thermography [5, 6].

The accent in this paper is on the analysis of temperature signals in corroded metals and the development of a robust inversion algorithm which would be independent of absorbed energy and image observation time.

2. INFORMATIVE PARAMETERS

The following parameters have been proposing in thermal NDT in order to detect and characterise internal defects:

(1) temperature increase $T(i,j,\tau)$ (referred also as excess temperature) where (i,j) specify geometric coordinates of each surface point in a IR image and τ-time;

†Author to whom correspondence should be addressed.

NOMENCLATURE

NDT nondestructive testing
IR infra-red
T temperature (absolute or above ambient) [°C or K]
T_{max} maximum excess specimen temperature (at the end of heating) [°C or K]
T_{min} minimum excess specimen temperature (at the end of adiabatic process) [°C or K]
$C = \Delta T/T$ temperature contrast over defect
L specimen thickness [m]
$\lambda = \Delta L/L$ material loss due to corrosion
D_d diameter of corroded area [m]
K conductivity [W mK^{-1}]
W absorbed energy density [J m^{-2}]
Q absorbed power density [W m^{-2}]
$Fo = \alpha\tau/L^2$ dimensionless time (Fourier number)
$Fo_h = \alpha\tau_h/L^2$ dimensionless heat pulse duration.

Greek symbols
α diffusivity [m^2 s^{-1}]
ΔT temperature signal over defect [°C or K]
Θ_D dimensionless temperature for Dirac pulse
Θ_{SP} dimensionless temperature for square pulse
τ time [s]
τ_{obs} observation time [s]
τ_h heating time [s].

(2) temperature signal $\Delta T(i,j,\tau)$, or difference between temperature in each pixel and reference temperature specified by an operator in a single image or in a sequence of images: $\Delta T(i,j,\tau) = T(i,j,\tau) - T(i_{ref},j_{ref},\tau)$;

(3) temperature contrast $C(i,j,\tau) = \Delta T(i,j,\tau)/T(i,j,\tau)$; another expression for the so called normalised temperature contrast is $C^*(i,j,\tau) = \Delta T(i,j,\tau)/T(i,j,\tau_{ref})$, where the reference time could be chosen in suitable point of time evolution curve, e.g. when the temperature in a particular pixel becomes maximum, or at the beginning of a process when the influence of uneven heating is the most noticeable and

(4) specific heat transit time τ^* when temperature $T(i,j,\tau)$ reaches the predetermined value.

In this research we deal with the measurement of temperature contrast affected by variations in the specimen's thickness. This parameter does not depend on the absorbed energy and it could be easily determined in computerised thermographic systems.

3. MODELS OF THE CORRODED SPECIMEN

Corrosion measurement is generally reduced to the measurement of a wall thickness. Some real corrosion situations are shown in Fig. 1(a). The mathematical simulation of corrosion areas of such shapes are possible in 3D space by computing a grid with an extremely large number of nodes.

The most reasonable practical approximation of the situations in Fig. 1(a) could be made in 3D Cartesian coordinates where the corrosion defects are modelled with air-filled parallelepipeds on the rear surface of a specimen [7] [Fig. 1(b)]. In many cases, corrosion spots could be simulated with disk-shape defects in 2D cylindrical coordinates [Fig. 1(c)], essentially reducing computation time. Channel-like defects could be modelled in 2D Cartesian space [Fig. 1(d)], but this model has no advantages in computation time when compared with the model of Fig. 1(c). Finally, large-size corrosion areas lead to 1D Cartesian geometry where thermal processes occur independently in non-defect and defect areas. It is important to underline that in the 1D model, the 3D heat diffusion effects are neglected and characterisation results will not be accurate upon the defect edges. The model in Fig. 1(c) is believed to be the most convenient for developing the thermal characterisation algorithm. Below we combine the use of 1D and 2D models in order to derive practical inversion functions.

4. ANALYSIS OF 1D MODELS

4.1. *Basic expressions*

Heating a thin metal slab with a short heat pulse could be considered as an adiabatic process. The temperature history on the heated surface is described in the 1D case with the following equations [8]:

for Dirac pulse (pulse duration is neglected)

$$\Theta_D = \frac{T(\tau,L)}{W\alpha/KL} = 1 + 2\sum_{n=1}^{\infty}\exp(-n^2\pi^2 Fo) \quad Fo = \frac{\alpha\tau}{L^2} \tag{1}$$

during a square pulse of duration τ_h

$$\Theta_{SP} = \frac{T(\tau,L)}{QL/K} = Fo + \tfrac{1}{3} - \frac{2}{\pi^2}\sum_{n=1}^{\infty}\frac{1}{n^2}\exp(-n^2\pi^2 Fo) \tag{2}$$

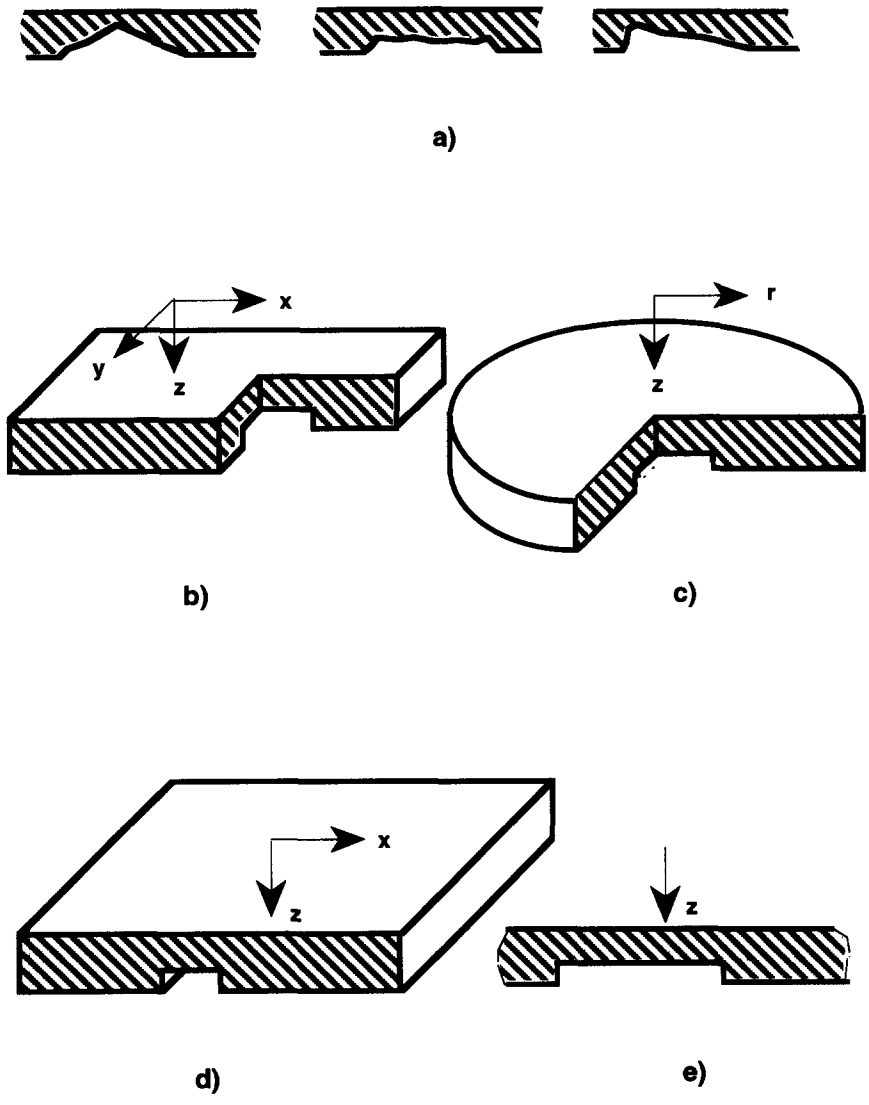

Fig. 1. Corrosion models; (a) real situation, (b) 3D Cartesian geometry, (c) 2D cylindrical geometry, (d) 2D Cartesian geometry and (e) 1D Cartesian geometry.

after square pulse

$$\Theta_{SP} = \frac{T(\tau, L)}{QL/K}$$

$$= Fo_h + \frac{2}{\pi^2}\sum_{n=1}^{\infty}\frac{1}{n^2}\exp(-n^2\pi^2 Fo)$$

$$\times[\exp(n^2\pi^2 Fo_h) - 1] \quad Fo_h = \frac{\alpha\tau_h}{L^2}. \tag{3}$$

Equation (1) is simpler but it is valid for times when $\tau \gg \tau_h$ and does not provide the temperature at the end of heating. In the analysis below we use equations (2) and (3) which allow one to analyse the whole process after having turned on the heater with the square pulse. It is worth mentioning that flash tubes do not provide an exactly square pulse but, unless dealing with temperature during the pulse, we consider this to be a second order effect.

4.2. *Square-pulse heating of a plate*

It is obvious from equation (3) that temperature values depend on three combinations of parameters: QL/K; $Fo_h = \alpha\tau_h/L^2$; $Fo = \alpha\tau/L^2$. The first group of parameters is responsible for absorbed energy, the second group relates to heating pulse and the third one specifies dimensionless time. As we mentioned

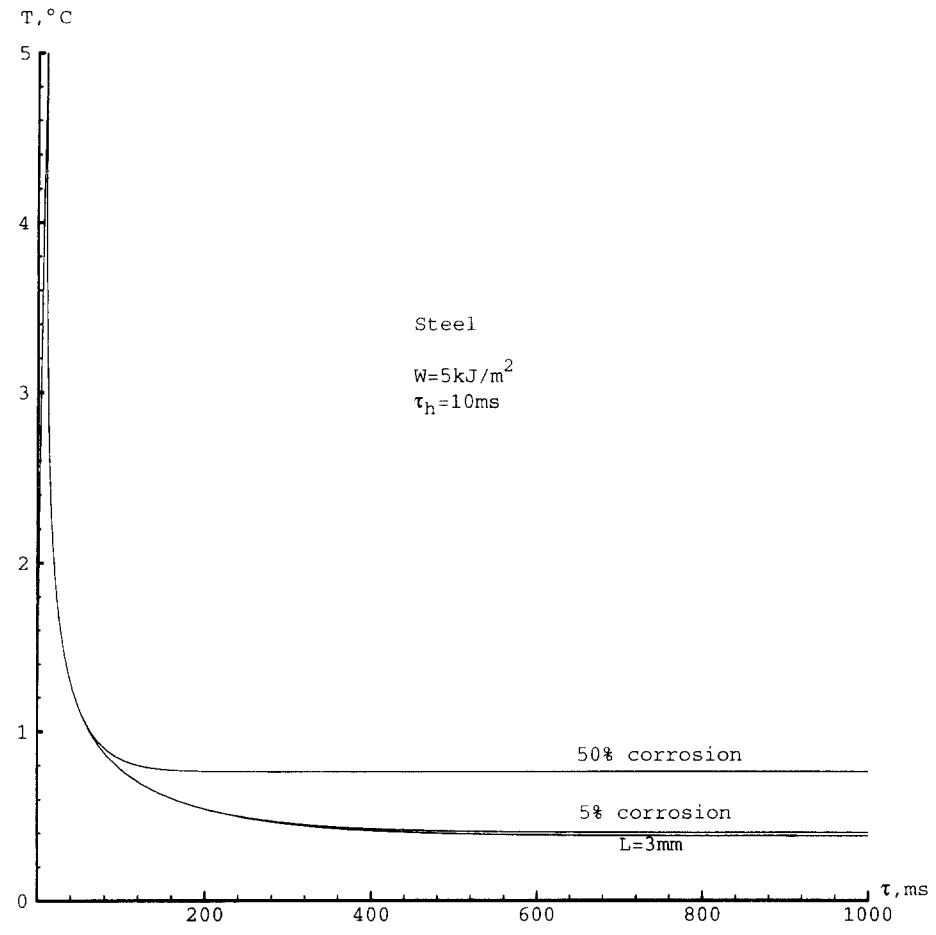

Fig. 2. Temperature evolution functions in square pulse heating of steel specimen: heating-cooling stage.

above, corrosion decreases the specimen thickness L, influencing all three groups of parameters. An example of a whole temperature evolution curve is presented in Fig. 2 for a steel specimen (thickness $L = 3$ mm; conductivity $K = 32$ W mK^{-1}; diffusivity $\alpha = 73.2 \times 10^{-7}$ m^2 s^{-1}) heated with the square pulse of duration $\tau_h = 10$ ms. Besides the "basic" curve, there are two temperature evolution curves for the same specimen with thickness 1.5 and 2.85 mm that corresponds to 50 and 5% material loss, respectively. It is seen that excess temperature on the surface reaches the maximum value of 5°C at the end of the pulse with an absorbed energy $W = 5$ kJ m^{-2} decreasing rapidly during some tens of milliseconds after the pulse. The two curves describing sound and corroded areas start to diverge at about 100 ms, giving an idea of the best observation time. For smaller material loss the best observation time moves toward a longer time (about 300 ms for 5% material loss). It is also important that results in Fig. 2 correspond to the 1D case. For real 3D defects it is expected that the temperatures in both defect and sound areas come together again, decreasing up to ambient temperature.

Another conclusion coming from functions plotted in Fig. 2 is that after a fast temperature decrease there is a rather long stage when the temperature in both defect and non-defect areas does not vary much. In "adiabatic heating" the dimensionless temperature at the end of the process is given by the expression $TK/QLFo_h$. In a real case, the specimen temperature decreases slowly to the ambient level. It is important to realise that corrosion detection has to be made during this relatively long period when the excess temperature of a specimen is not very high and therefore the temperature resolution of the IR imager must be rather good.

The influence of a dimensionless heat pulse duration on the behaviour of a basic function is illustrated with graphs in Fig. 3, where temperature is normalised by QL/K value.

4.3. *Maximum and minimum temperatures*

Using some flash tubes simultaneously, it is possible to obtain the value $W \approx 60$ kJ m^{-2}. In this case the excess specimen temperature could reach some tens of degree centrigrade (see Fig. 2). In a general case both the maximum temperature T_{max} and the ratio between maximum and minimum temperature $m_{max} = T_{max}/T_{min}$ depend on the pulse duration. This statement is strictly correct only in adiabatic case where

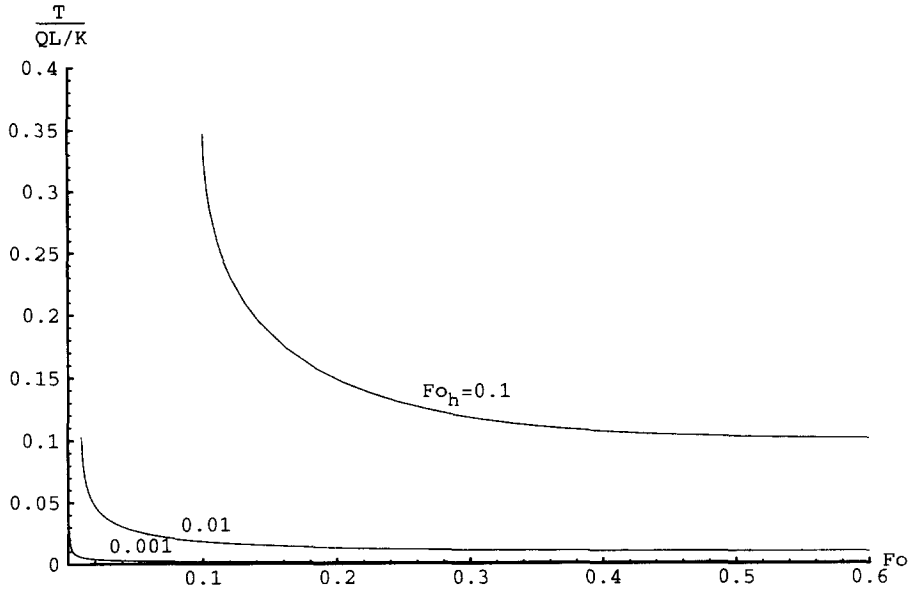

Fig. 3. Temperature decrease after square pulse heating.

$T_{min} = (QL/K)Fo_h$, but it is also useful in practice. The corresponding values given by equations (4) are presented in Table 1:

$$T_{max} = \frac{QL}{K}\left\{Fo_h + \frac{2}{\pi^2}\sum_{n=1}^{\infty}\frac{1}{n^2}[1-\exp(-n^2\pi^2 Fo_h)]\right\}$$

$$m_{max} = T_{max}/T_{min} = 1 + \frac{2}{\pi^2 Fo_h}\sum_{n=1}^{\infty}\frac{1}{n^2}[1-\exp(-n^2\pi^2 Fo_h)]. \quad (4)$$

It is seen from Table 1 that shorter pulses provide a larger ratio between the maximum and minimum excess temperatures due to the fact that during a short pulse only near-surface layers are heated and in the cooling stage in-depth heat dissipation is stronger than after a longer pulse.

For dependence m_{max} vs Fo_h, we found the following expression using least-squares fits: $m_{max} = 1.118/\sqrt{(Fo_h)}$.

When adopting an adiabatic model there is a particular time when the difference between the surface temperature and the value $T_{min} = (QL/K)Fo_h$ becomes less than any pre-determined small value I which specifies in fact how close is the temperature to its adiabatic limit. It is natural to determine the "end time" of the process Fo_{end} via the following transcendent equation: $I = [T(Fo_{end}) - T_{min}]/T_{min}$.

Values of Fo_{end} for various values of Fo_h and I are given in Table 2.

5. THERMAL PROPERTIES OF STEEL SPECIMEN IN CORROSION DETECTION

Thermal properties of various types of steel are specified in Table 3.

Three types of steel could be specified by thermal conductivity and diffusivity:

Type 1:

$K = 16.3\,\mathrm{W\,mK^{-1}}$; $\alpha = 44.4\times10^{-7}\,\mathrm{m^2\,s^{-1}}$

Type 2:

$K = 32.0\,\mathrm{W\,mK^{-1}}$; $\alpha = 73.2\times10^{-7}\,\mathrm{m^2\,s^{-1}}$

Type 3:

$K = 62.0\,\mathrm{W\,mK^{-1}}$; $\alpha = 176.3\times10^{-7}\,\mathrm{m^2\,s^{-1}}$.

If the specimen thickness varies from 1 to 5 mm and the heating duration is 5 ÷ 10 ms, the corresponding Fo_h values are in the range from 0.0008 to 0.15.

Table 1. Maximum temperature at the end of square-pulse heating and ratio between maximum and minimum temperatures

Dimensionless heat pulse duration, Fo_h	Maximum temperature at the end of heating, $T_{max}(Fo_h)/(QL/K)$	Ratio $m_{max} = T_{max}/T_{min}$
0.001	0.0357	35.6825
0.005	0.0798	15.9577
0.010	0.1128	11.2838
0.050	0.2523	5.0463
0.100	0.3568	3.5683

Table 2. End time of thermal process

Heat pulse duration, Fo_h	End time Fo_{end}		
	$I = 0.01$	$I = 0.05$	$I = 0.10$
0.001	1.457	1.142	0.960
0.005	1.461	1.146	0.966
0.010	1.465	1.152	0.973
0.050	1.498	1.199	1.030
0.100	1.540	1.258	1.102

Table 3. Thermal properties of steel [11]

Steel	Conductivity, K [W mK^{-1}]	Diffusivity, α [m^2 s^{-1}]
18% Cr, 8% Ni	16.3	44.4×10^{-7}
10 ÷ 50% Ni	14 ÷ 26	$(36.1 \div 72.0) \times 10^{-7}$
10 ÷ 30% Cr	19 ÷ 31	$(54.2 \div 86.7) \times 10^{-7}$
0.5 ÷ 1.5% C	36 ÷ 54	$(97.0 \div 147.4) \times 10^{-7}$
2% Mn	38	105.0×10^{-7}
2% W	62	176.3×10^{-7}

Absorbed energy for black-painted specimens could vary by our estimates from 1 to 60 kJ m^{-2}, depending on the type and number of flash tubes used.

6. GENERAL SENSITIVITY TO MATERIAL LOSS

By using the term "sensitivity to material loss" we assume that there is absolute or relative temperature increase in the corroded area for each 1% of material loss. This could be expressed by the following function:

$$\frac{\Delta T/T}{\Delta L/L} = 1 - 2Fo_h \times \frac{1 + 2\sum_{n=1}^{\infty} \{\exp[n^2\pi^2(Fo_h - Fo)] - (Fo/Fo_h)\exp(-n^2\pi^2 Fo) \times [\exp(n^2\pi^2 Fo_h) - 1]\}}{Fo_h + (2/\pi^2)\sum_{n=1}^{\infty} \frac{1}{n^2}\{\exp(-n^2\pi^2 Fo) \times [\exp(n^2\pi^2 Fo_h) - 1]\}} \quad (5)$$

A graph of equation (5) is presented in Fig. 4 for various heat pulse duration. The following conclusions could be made from Fig. 4.

(1) A negative sign of presented function means that an increase in thickness leads to a decrease in temperature and vice versa.

(2) Sensitivity to thickness variation depends on time: it is very low in the beginning of the process (when the thermal front has not yet reached the rear surface, if we use thermal wave terminology) and it is at maximum at the end of the process (1% of temperature increase per 1% of thickness decrease). Again, taking into account the blurring effect of 3D heat diffusion, there must be an optimum period for corrosion detection.

7. ANALYSIS OF 2D MODELS AND LIMITS OF 1D SOLUTIONS

7.1. *Temperature signals over disk-shape defects*

The heat diffusion around defects decreases temperature signals and shortens the best observation time. It could be expected that the shorter the observation time, the more accurate the corrosion measurements from the point of view of 3D heat transfer phenomena, but unfortunately, the general sensitivity to rear-side corrosion decreases for the shorter time (see Fig. 4). Hence the optimum observation time is the compromise between these two factors.

In order to determine the limits of 1D approach, we calculated twenty variants of practical inspection situations for steel specimens with thickness 3 mm, using "Termo.Heat" software (Tomsk Polytechnic University, Russia). The diameters of the disk-shape defects D_d varied from 10 to 60 mm, and the loss of material varied from 5 to 50%. The calculated values of the temperature signals for the absorbed energy 60 kJ m^{-2} and the temperature contrasts are presented in Table 4 for various observation times. The end of the thermal process may be observed more or less after 1000 ms from the heat stimulus.

The following conclusions could be made from Table 4.

(1) Temperature signals over defects increase fast immediately after the heat pulse, reach their maximum

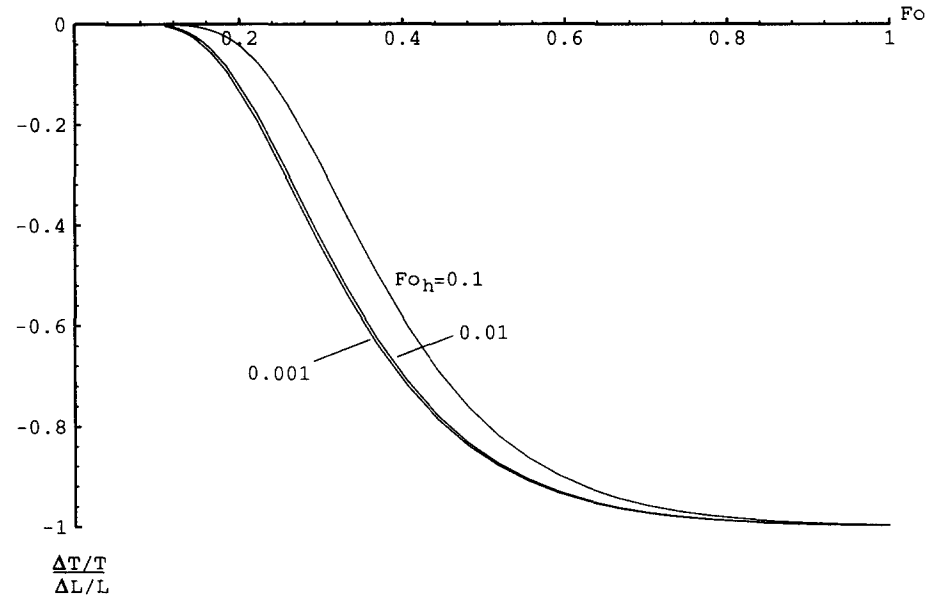

Fig. 4. Sensitivity of thermal NDT to specimen thickness variation.

values, and then start to decrease slowly due to 3D heat diffusion effects.

(2) For a short observation time, the defect diameter does not influence the measured parameters.

(3) The choice of an optimum observation time depends on the acceptable level of both absolute signals and contrasts. For instance, on one hand it is obvious that for IR imagers with temperature resolution 0.1°C, the detection of 5% corrosion is possible only after 360 ms (for larger defects the optimum observation time moves to shorter values). On the other hand, it was shown elsewhere that in practice, even black-painted surfaces provide a noise contrast level not less than 2%. It means that corrosion in the range of material loss from 5 to 50% could be reliably detected at times longer than 360 ms when temperature contrasts in corroded areas become more than 2%.

(4) Data in Table 4 could be also interpreted for inversion purposes due to the evident connection between temperature contrast and material loss.

(5) Defects with diameters of more than 40 mm

Table 4. Calculated parameters of thermal inspection of corrosion in steel ($L = 3$ mm; $K = 32$ W mK^{-1}; $\alpha = 73.2.\ 10^{-7}$ m^2 s^{-1}; $\tau_h = 10$ ms; $W = 60$ kJ m^{-2})

$\Delta L/L$	D_d [mm]	$\Delta T/T$ 90 [ms]	360 [ms]	840 [ms]	1000 [ms]	ΔT [°C] 90 [ms]	360 [ms]	840 [ms]	1000 [ms]
0.5	60	0.052	0.765	0.979	0.983	0.517	3.890	4.425	4.427
	40	0.052	0.765	0.979	0.983	0.517	3.890	4.425	4.427
	20	0.052	0.765	0.960	0.947†	0.517	3.889	4.339	4.267†
	10	0.052	0.720	0.663†	0.591†	0.517	3.664	2.997†	2.663†
0.3	60	0.003	0.294	0.433	0.436	0.028	1.504	1.982	1.988
	40	0.003	0.294	0.433	0.436	0.028	1.504	1.982	1.988
	20	0.003	0.294	0.427	0.422†	0.028	1.504	1.952	1.928†
	10	0.003	0.280	0.304	0.273†	0.028	1.433	1.392†	1.245†
0.2	60	0.0004	0.144	0.244	0.246	0.004	0.735	1.115	1.122
	40	0.0004	0.144	0.244	0.246	0.004	0.735	1.115	1.122
	20	0.0004	0.144	0.240	0.239†	0.004	0.735	1.100	1.091†
	10	0.0004	0.138	0.173	0.156†	0.004	0.703	0.791	0.711†
0.1	60	0.0000	0.055	0.113	0.115	0.000	0.279	0.512	0.519
	40	0.0000	0.055	0.113	0.115	0.000	0.279	0.512	0.519
	20	0.0000	0.055	0.112	0.112	0.000	0.279	0.505	0.505
	10	0.0000	0.053	0.081	0.074†	0.000	0.267	0.365	0.331†
0.05	60	0.0000	0.025	0.054	0.055	0.000	0.128	0.246	0.250
	40	0.0000	0.025	0.054	0.055	0.000	0.128	0.246	0.250
	20	0.0000	0.025	0.053	0.053	0.000	0.128	0.243	0.243
	10	0.0000	0.024	0.038	0.035†	0.000	0.122	0.175	0.159†

†Signal decreased because of 3D heat diffusion.

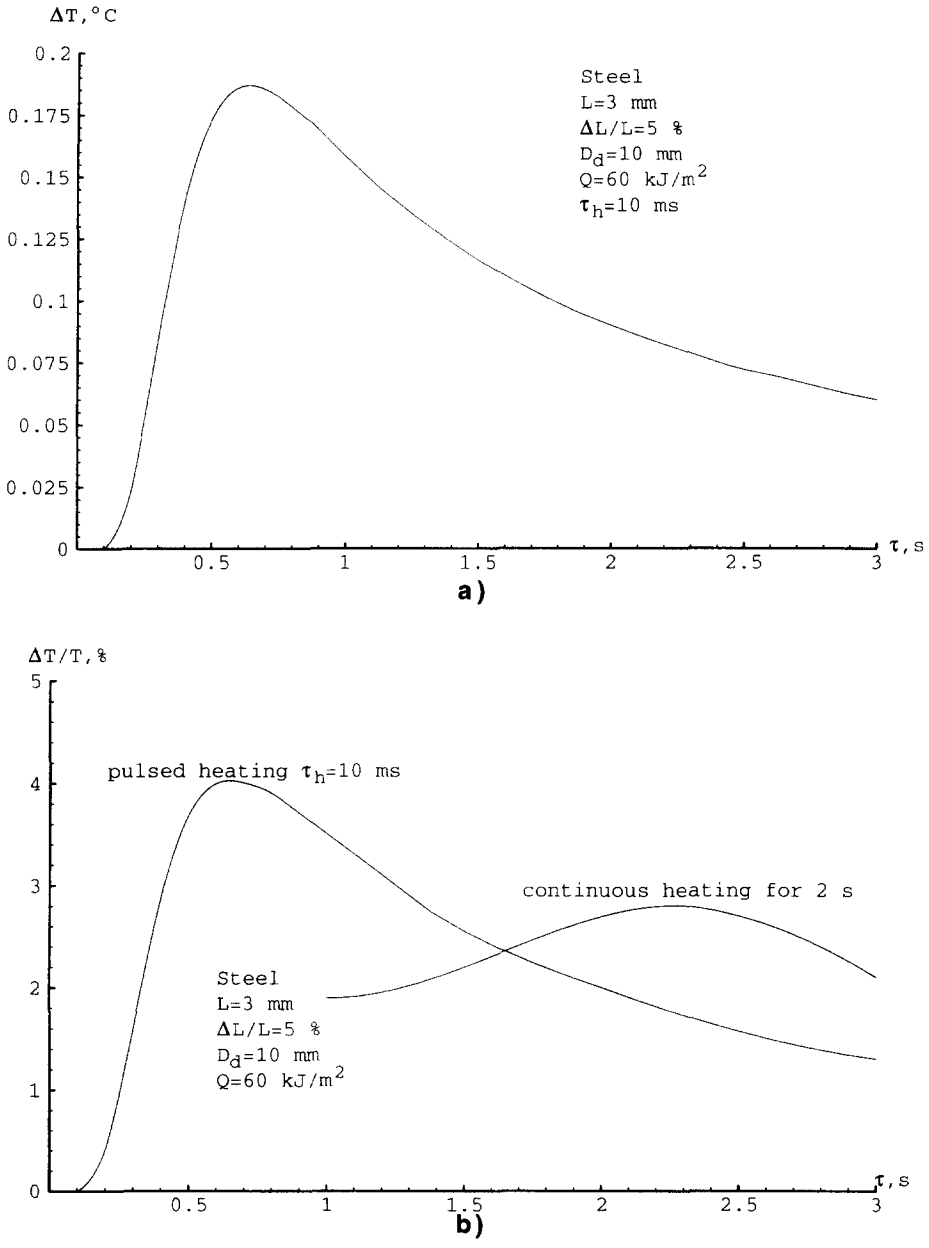

Fig. 5. Temperature signal (a) and contrast (b) vs time for 5% corrosion with diameter 10 mm in steel (type II).

could be regarded as 1D defects (i.e. having infinite planar size). The influence of 3D effects for small-size (5%) corrosion defects in steel specimens of thickness 3 mm is shown in Fig. 5 for both temperature signal and contrast. It is clearly seen that the period from 300 to 1300 ms could be approximately recommended to detect this kind of defect. Moreover, during this period image averaging is strongly recommended in order to increase the signal-to-noise ratio (SNR) of the IR system (up to 30 images could be averaged during 1 s providing a five-fold increase in SNR for IR imagers with a frame frequency 30 Hz). It is also important that for defects with larger diameters the temperature signals will exist even for a longer time.

(6) The general influence of 3D heat diffusion and respectively the limits of 1D solutions could be estimated by the ratio $k_{3D}(\tau) = \Delta T(D_d, \Delta L/L, \tau)/\Delta T(D_d \to \infty, \Delta L/L, \tau)$, which relates real defects to defects with infinite planar size. This coefficient vs time is shown in Fig. 6. It is seen that the model discussed could be regarded as a 1D model for times shorter than 240–280 ms with 5% accuracy and for times shorter than 280–440 ms with 10% accuracy.

Data of Figs. 5 and 6 illustrate that temperature

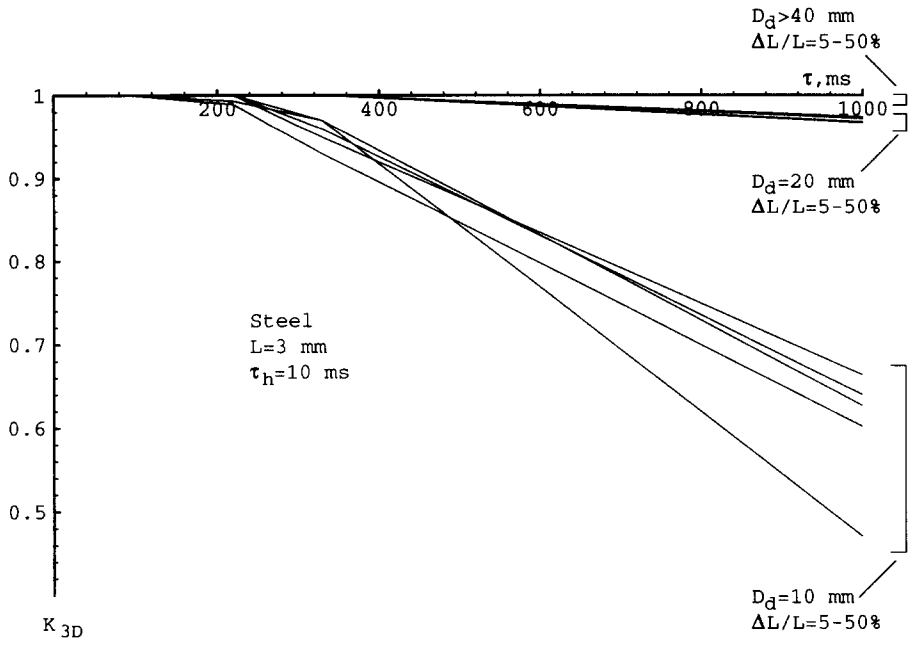

Fig. 6. 3D heat diffusion effects in thermal NDT of corrosion in steel (type II).

signals in steel exist for a time long enough to use modern IR imagers.

7.2. *Quasi-continuous heating*

In order to compare flash and quasi-continuous heating, the numerical model was used with heat pulses of duration 2 s and power $Q = 10\,000$ W m^{-2} (i.e. the absorbed energy in this case was 20 kJ m^{-2} against 60 kJ m^{-2} accepted for short pulse heating in Fig. 5). In Fig. 5 it is shown as the maximum temperature contrast over a corroded area with a diameter of 10 mm and material loss of 5%, occurred at 380 ms after the end of heating, reaching the value of 2.8%. In the case of a short pulse heating excitation of the same sample, the maximum of the contrast arrives at 4%, but occurring earlier. The maximum temperature signal was 0.043°C against 0.19°C for flash heating. Detailed discussion of this phenomenon is beyond this report. Nevertheless, it is worth mentioning that the effectiveness of the heating technique depends mainly on the type of noise which dominates in a particular experiment [9]. Usually, in tests with IR imagers of higher quality, the surface multiplicative noise is more than the additive noise of the camera itself, electronics, etc. In this case the maximum SNR value occurs for the maximum temperature contrast. Hence, flash heating will provide a more reliable detection of defects.

8. INVERSION EXPRESSION

We assume that corrosion by-products do not modify significantly thermal properties of metal. With such a hypothesis, corrosion is equivalent only to thickness variation. It means that the temperature in both sound and corroded areas could be described with the same equations (2) and (3). Let us specify the relative loss of material due to corrosion as $\lambda = \Delta L/L$. We assume that the inversion algorithm will involve only decreasing temperature (at the cooling stage of the thermal process). Then, using equation (3), it is possible to obtain the following expression, which connects the measured temperature contrast to material loss:

$$F = \frac{T(\tau, L-\Delta L) - T(\tau, L)}{T(\tau, L)} = \frac{1}{1-\lambda}$$

$$\left\{1 + \frac{2}{\pi^2 Fo_h \dfrac{1}{(1-\lambda)^2}} \sum_{n=1}^{\infty} \frac{1}{n^2} \times \left[\exp\left(-n^2\pi^2 Fo \frac{1}{(1-\lambda)^2}\right) \times \left(\exp\left(n^2\pi^2 Fo_h \frac{1}{(1-\lambda)^2}\right) - 1\right)\right]\right\}$$

$$\times \frac{}{\left\{1 + \dfrac{2}{\pi^2 Fo_h} \sum_{n=1}^{\infty} \dfrac{1}{n^2} [\exp(-n^2\pi^2 Fo) \times (\exp(n^2\pi^2 Fo_h) - 1)]\right\} - 1.} - 1. \quad (6)$$

It is important to note that function F depends on time, the type of material and material loss. For measurement of corrosion we need the inversion func-

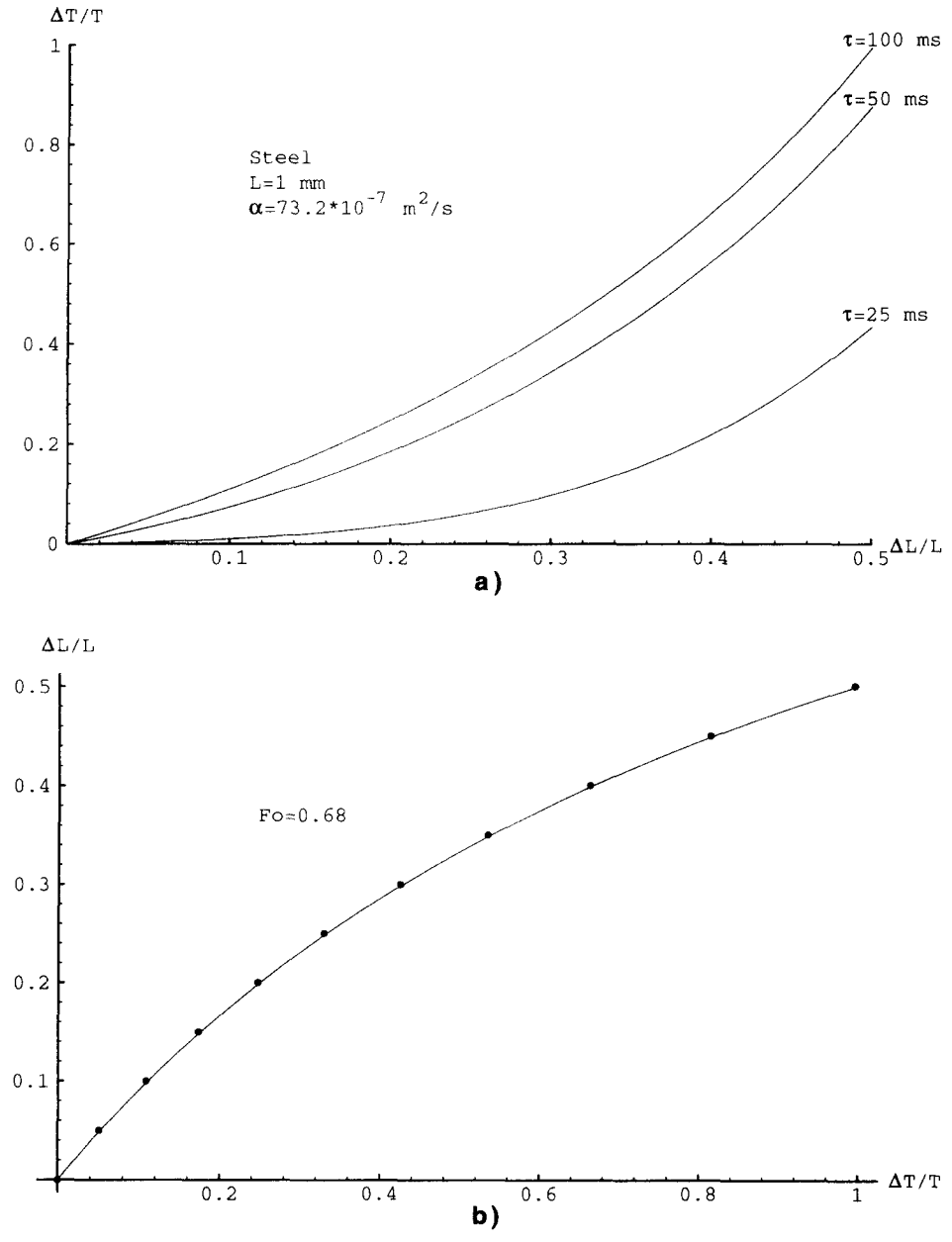

Fig. 7. Inversion functions in corrosion detection; (a) temperature contrast vs material loss for steel and (b) inversion function for $Fo = 0.68$.

tion F^{-1}, which will connect the material loss to the measured temperature contrast.

Function F is presented in Fig. 7(a) for a steel specimen of 1 mm thickness at three observation times: 20, 50 and 100 ms. It is well seen that higher sensitivity to thickness variation occurs at longer times (the same conclusion was earlier made from Fig. 4).

We assume that the simplest inversion function should be derived at the end of the process when the sensitivity to the thickness variation is maximum and 3D heat diffusion effects are not too strong. We found that the Fourier number $Fo = 0.68$, which corresponds to the 70% of the end process time ($I = 10\%$), would be convenient for inversion purposes. Heat pulse duration is recommended to be chosen as $Fo_h = 0.01$, i.e. in the middle of the range of possible practical values. The choice of a particular value of Fo_h is made after the analysis of its influence on an observation time which showed that for rather short heat pulses this influence could be neglected. The appearance of the inversion function F^{-1} is shown in Fig. 7(b) with some numerical points which have been

inverted from equation (6). Using least-squares fit we approximated the inversion function with the following analytical function:

$$\Delta L/L = \frac{\Delta T/T}{1+\Delta T/T} \tag{7}$$

or

$$\Delta L/L = 1 - T(i_{ref}, j_{ref}, \tau_{obs})/T(i, j, \tau_{obs}). \tag{8}$$

This inversion formula could be obtained also directly from equation (3) if $\tau \to \infty$. Its verification for various materials and thicknesses, as well as for possible variations in observation times, is performed below theoretically and experimentally. Here we state that equation (7), being originally derived for steel specimens with the above specified thermal properties, does not depend on the type of material and heat pulse duration; it could be recommended to be used for a wide range of materials if the thermal properties are a priori known and respective observation times are previously determined.

Approximated values of recommended observation time τ_{obs} are presented in Table 5 for various steel specimens.

Table 5. Recommended observation time in corrosion detection for steel specimens ($Fo = 0.68$)

Steel	L [mm]	τ_{obs} [ms]
Type I Low-conductive	1	150
	3	1380
	5	3830
Type II Medium-conductive	1	95
	3	840
	5	2320
Type III High-conductive	1	40
	3	350
	5	960

9. THEORETICAL VERIFICATION OF INVERSION FUNCTIONS

We used the calculated values of temperature contrasts over defects of various diameter in steel specimen of thickness 3 mm as input parameters in corrosion detection using equation (7). Inversion results for material loss $\Delta L/L$ together with error values defined by evident expression $(\Delta L/L_{true} - \Delta L/L_{inv})/\Delta L/L_{true}$ are presented in Table 6.

The use of equation (7) requires *a priori* knowledge of specimen thermal properties and thickness to determine the optimum observation time. If the thickness of a specimen under test is usually known with good accuracy, the values of thermal properties are to be measured or borrowed from corresponding handbooks with possible errors. The influence of discussed parameters could be analysed using the obvious expression which connects errors in specifying observation time, diffusivity and thickness: $Fo = \alpha\tau/L^2$; $\Delta Fo/Fo = (\Delta\alpha/\alpha) + (\Delta\tau/\tau) - 2(\Delta L/L)$.

The last equation illustrates that a 1% error in time measurement is equivalent to a 1% error in the specification of diffusivity or a 0.5% error in specifying thickness. In a real experiment the observation time would be determined with accuracy which is limited with frame (or line) time. From this point of view, the IR imagers with high frame frequency are to be

Table 6. Inversion results in corrosion detection (steel specimen: $L = 3$ mm; $K = 32$ W mK^{-1}; $\alpha = 73.2.\ 10^{-7}$ m^2 s^{-1}; $\tau_h = 10$ ms; $Q = 50$ kJ m^{-2})

True value of $\Delta L/L$	D_d [mm]	Inversion results for $\tau_{obs} = 840$ ms		
		$\Delta T/T$	$\Delta L/L$	Error [%]
0.5	60	0.979	0.495	1.06
	40	0.979	0.495	1.06
	20	0.960	0.490	2.04
	10	0.663	0.400	20.26
0.3	60	0.433	0.307	−2.33
	40	0.433	0.307	−2.33
	20	0.427	0.299	−0.26
	10	0.304	0.233	22.29
0.2	60	0.244	0.196	1.93
	40	0.244	0.196	1.93
	20	0.240	0.194	3.23
	10	0.173	0.147	26.25
0.1	60	0.113	0.102	−1.53
	40	0.113	0.102	−1.53
	20	0.112	0.101	−0.72
	10	0.081	0.075	25.07
0.05	60	0.054	0.051	−2.47
	40	0.054	0.051	−2.47
	20	0.053	0.050	−0.66
	10	0.038	0.037	26.78

used in corrosion detection. We found that a variation in observation time of about 30–40 ms (frame frequency 30–25 Hz) leads to an error in material loss measurement of some percent. Consequently, inaccuracy in specifying the diffusivity value of about 10%, expected in practice, will cause a detection error of some percent. An error in specifying the L value in order of some percent does not affect much testing results.

Finally, we have performed a numerical simulation to study the sensitivity of the corrosion measuring to input parameters errors. The following values which could happen in practice have been chosen: $L = 1$ mm; $K = 16.3$ W mK^{-1}; $\alpha = 44.4 \times 10^{-7}$ m^2 s^{-1}; $\tau_h = 5$ ms; $\Delta L/L = 20\%$. Input data were deliberately distorted, but affecting the result in one direction, i.e. not compensating each other. When performing the inversion, we decreased the thickness by 2%, increased the diffusivity by 10% and accepted an observation time of 30 ms less than predicted by the inversion formula (considering an IR imager with a 30 Hz frame frequency). In total, the determined observation time, 120 ms, was 50 ms less than the correct value (170 ms) which would be obtained with true input parameters. As a result, the predicted material loss (18.2%) was just 9.6% less than true value (20%).

10. EXPERIMENTAL VERIFICATION OF INVERSION FUNCTIONS

A sequence of IR images recorded in the corrosion detection test with the "Bales" IR imager has been used to verify the inversion function for $Fo = 0.68$. A

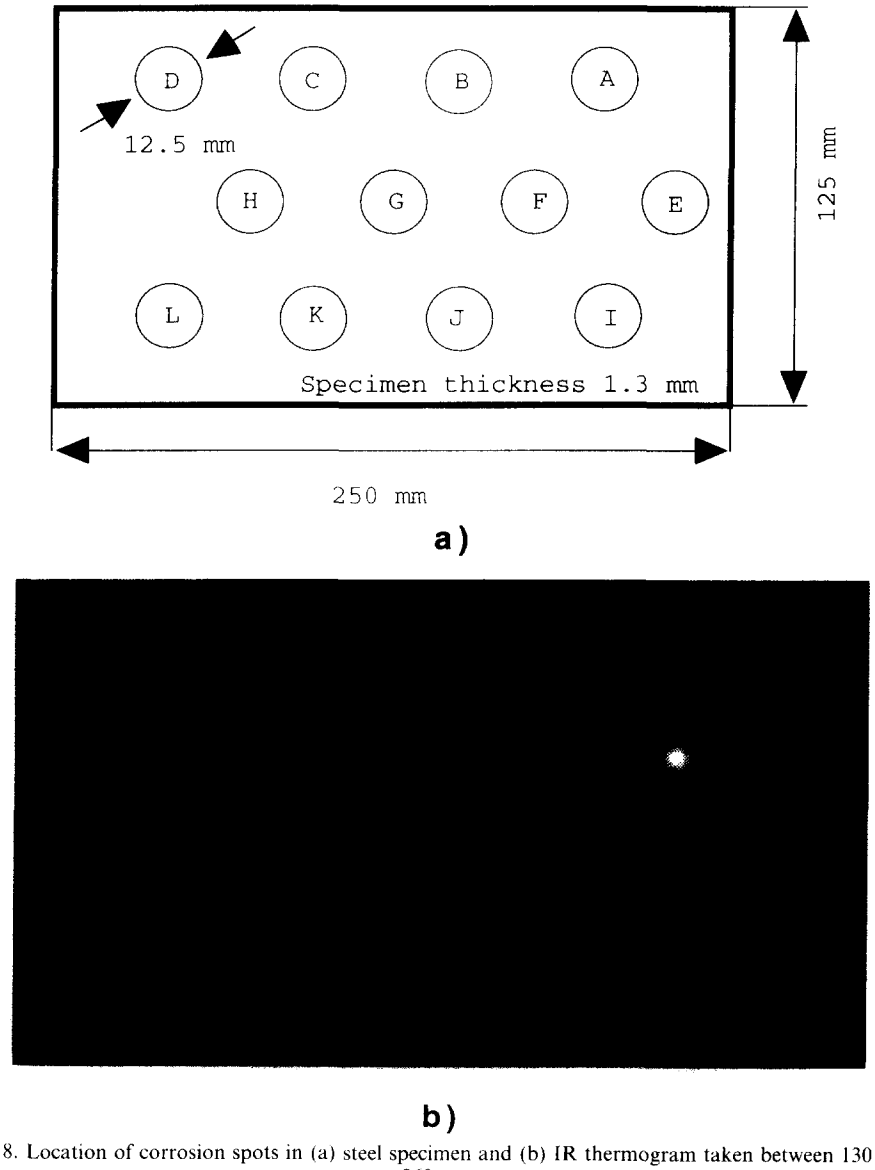

Fig. 8. Location of corrosion spots in (a) steel specimen and (b) IR thermogram taken between 130 and 260 ms.

Table 7. Description of simulated corrosion in steel specimen [Fig. 8(a)] and inversion results

Defect	Material loss, $\Delta L/L$ [%]	Temperature contrast, $\Delta T/T$ [%]	$\Delta L/L$ value after inversion of experimental data [%]	Inversion error [%]
A	2	11.9	10.6	430
B	8	16.7	14.3	78
C	14	31.4	23.9	71
D	20	39.7	28.4	42
E	26	37.5	27.3	5
F	36	72.4	42.0	16
G	36	65.4	39.5	10
H	42	75.4	43.0	2
I	48	99.1	49.8	4
J	54	150.0	60.0	11
K	62	262.0	72.4	17
L	74	440.0	81.5	10

steel specimen of thickness 1.3 mm was heated with two flash tubes for some centigrade above ambient temperature (heat pulse duration was 5 ms). Twelve bottom-hole defects, with a diameter of 12.5 mm simulated corrosion spots. Specifications of the defects are shown in Fig. 8(a) and in Table 7. Thermal properties of particular steel have been unknown and in accordance with data in Table 5, we have chosen the observation time between 130 and 260 ms after a heat pulse. Since the IR camera produced 1800 lines per second this time interval corresponded to the second recorded image. It is important to note that all empirical parameters which described the particular thermal test have been not well specified in order to simulate the practical case when only the inversion formula is used and the only verification criterion is error value $(\Delta L/L_{\text{true}} - \Delta L/L_{\text{inv}})/\Delta L/L_{\text{true}}$.

The thermal image of the steel specimen taken between 130 and 260 ms is shown in Fig. 8(b) [note that the locations of defects corresponds to those in Fig. 8(a)]. Taking into account the inevitable deterioration of image quality due to printing, we need to indicate that the experienced operator could distinguish up to ten defects (C–L) on an IR imager monitor. Of course, in our particular case, round shape of the defects and their regular locations help in their recognition, but the details of statistical defect detection are beyond the scope of present analysis. Thus, no special treatment of the image in Fig. 8(b) was performed due to the general good quality of

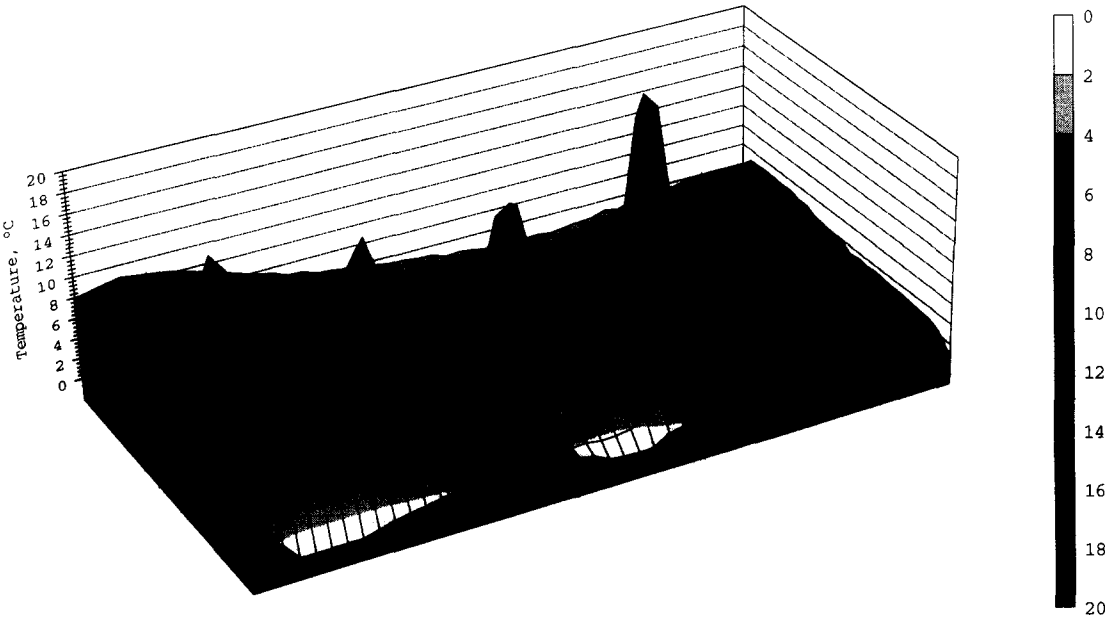

Fig. 9. 3D presentation of surface temperature for steel specimen with twelve corrosion spots [see Fig. 8(b)].

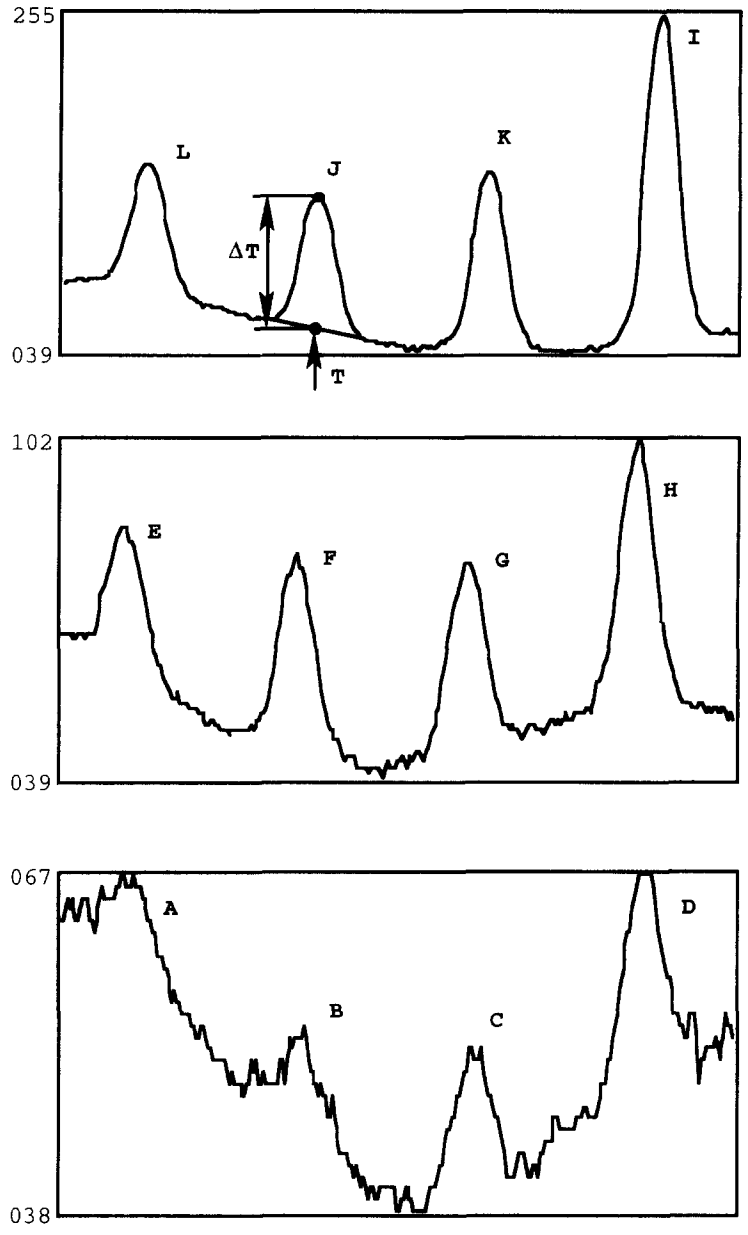

Fig. 10. Temperature profiles over corrosion spots in steel specimen [see Fig. 8(a)].

thermogram. Nevertheless, in order to be correct we need to say that careful analysis of this image with "look-up table" transformation revealed essential "prints" of two flash tubes on the left and right specimen edges that created problems in quantifying corrosion; more information on this is presented below.

Real excess temperature values are shown in Fig. 9 in temperature profiles–grey level presentation of the image from Fig. 8(b). It is seen that non-defect temperature varies from 2 to 10°C with a higher level in the left far corner where the thermal irradiation seemed to be more powerful.

The phenomena under discussion are clearly seen in temperature profiles traced through all defect areas (Fig. 10). The method of determining the temperature signals and contrasts is shown in the area of defect J. Note that the use of temperature contrasts allows one to process images not necessarily calibrated in real temperature but also in grey levels for not too high excess temperature, as illustrated in Fig. 10.

The inversion formula for $Fo = 0.68$ has been

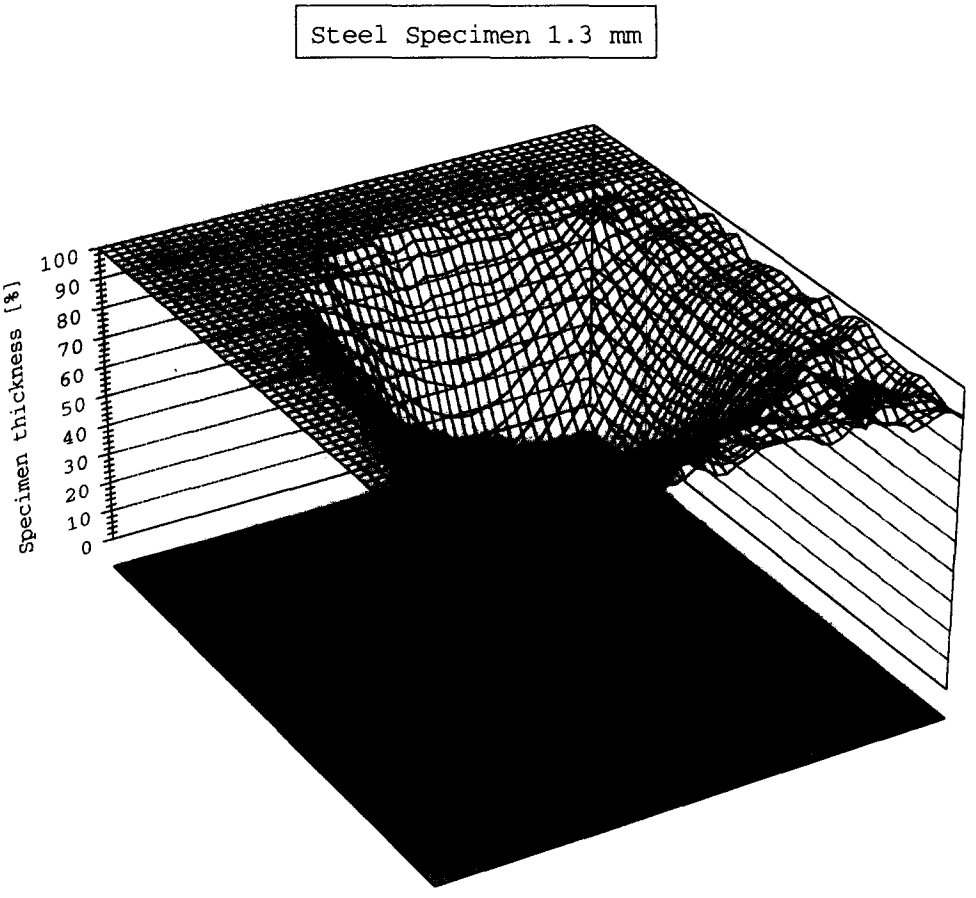

Fig. 11. Corrosion image for area with material loss 74%.

applied to each defect signal, with results presented in Table 7 (it is worth underlining that the inversion has been performed with 8-bit data using a straightforward calculation method that resulted, as we believe, in the worst accuracy to be obtained).

The main conclusions from the experimental verification of the inversion function are as follows:

(1) Inversion in the area of defect A with 2% of material loss produced the error of 430% because the signal from this defect is nearly lost on the background of noise and local heating non-uniformity. Hence, 2% corrosion could not be detected reliably and measured.

(2) Corrosion of about 8–14% (defects B,C) could be measured with 70–80% accuracy. This is probably low, even for approximate practical estimates.

(3) Corrosion of about 26–74% (defects D–L) could be measured with acceptable accuracy better than 17%.

(4) Material loss determined by the procedure above is overestimated in all cases that could not be random. We believe that this could be explained by overestimating the initial temperature [this temperature was measured in the "black" area around the specimen image in Fig. 8(b)].

11. SYNTHESIS OF "CORROSION IMAGE"

When the non-defect point or area is selected in the image, each pixel could be calibrated first in temperature contrast and then in material loss. It means that the initial IR image could be transformed into a "corrosion image". Three examples of such images are presented in Figs. 11–13.

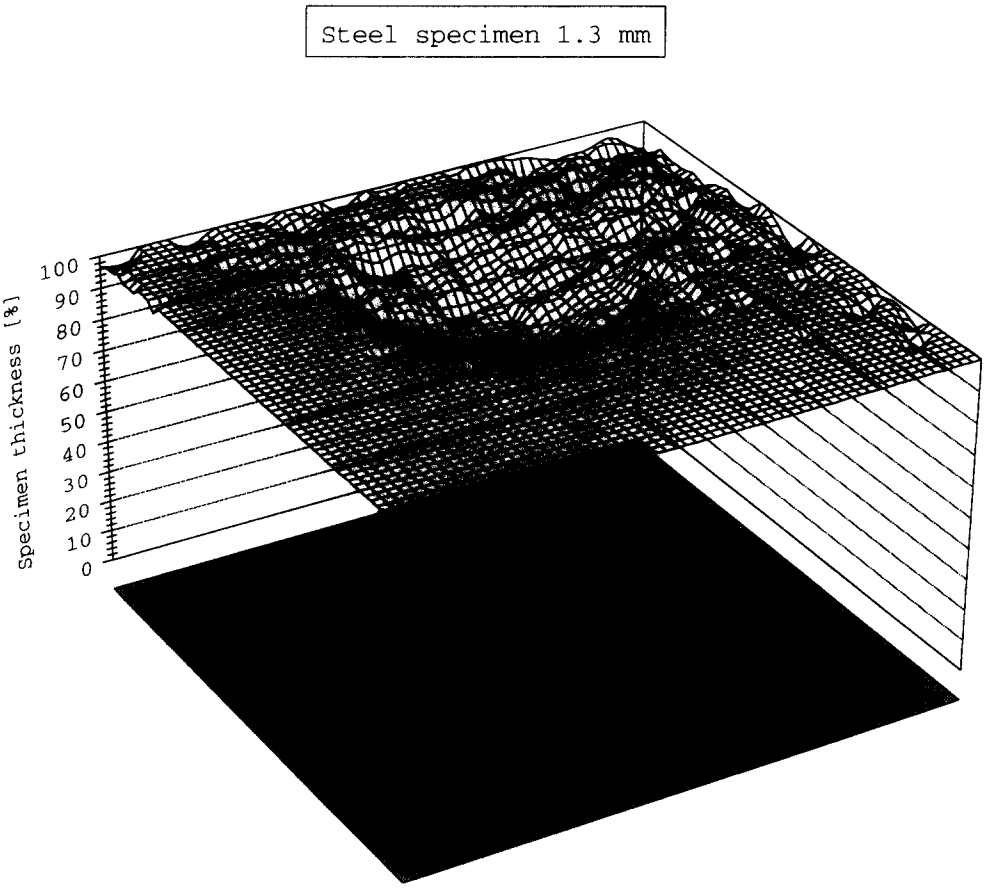

Fig. 12. Corrosion image for area with material loss 14%.

The most illustrative case of 74% corrosion (defect L) is shown in Fig. 11 where amplitude values are calibrated in the remaining material thickness and the decreasing signal in the area of defect shows clearly the material loss due to disk-shape corrosion.

Another case which is close to undetectable corrosion is shown in Fig. 12 for 14% of material loss (defect C).

Finally, the situation in Fig. 13 illustrates the appearance of minimum material loss (2%, defect A). It is seen that in this case the proposed procedure shows uneven heating rather than real corrosion, illustrating well the limit of the thermal method used.

The corrosion images in Figs. 11–13 illustrate another feature of the discussed algorithm. All quantitative inversion results will provide correct corrosion data only in the center of defect areas. This occurs due to a bell-shape decrease in temperature signal toward the edges, resulting in fact that corrosion will be underestimated in these areas. Some sophisticated algorithms to restore the real defect shape and size are under development now [10] but they are time-consuming and still not very reliable.

12. CONCLUSIONS

This paper contains the results of theoretical analysis for 1D and 2D models of corrosion. Most of the analytical expressions and graphs are presented in dimensionless form, allowing for expansion of the conclusions to any materials. Nevertheless, the accent in numerical examples is on corrosion detection in steel specimens of thickness from 1 to 5 mm. A simple inversion formula is proposed to process experimental IR images in order to determine material loss. As a final result, the "corrosion image" calibrated in material loss or in thickness of remained material could be synthesised using the proposed algorithm.

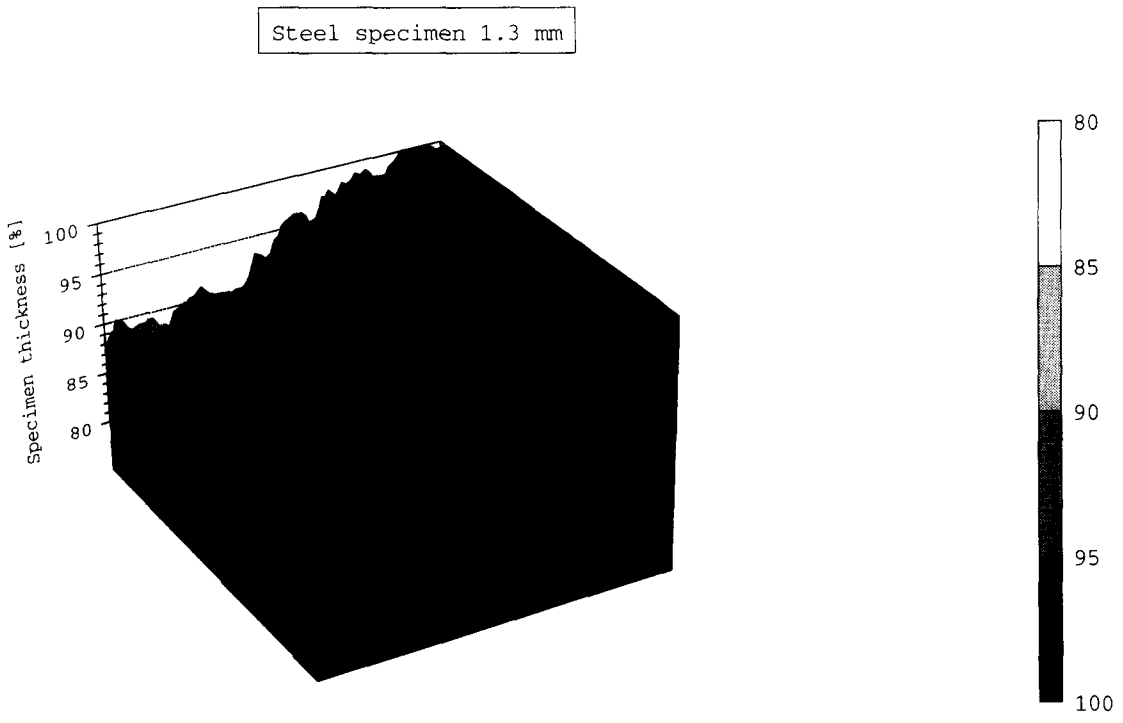

Fig. 13. Corrosion image for area with material loss 2%.

Verification of the inversion procedure has been made with the numerical 2D model and showed excellent convergence of data in the range of some percent. Furthermore, the straightforward use of the proposed algorithm to experimental IR images of corroded steel specimen proved its validity for material loss of more than 20%. Measurement error was not more than 17%, which is considered acceptable in practice.

The proposed testing technique is suitable for plastic materials as well.

REFERENCES

1. J. Alcott, An investigation of nondestructive inspection equipment: detecting hidden corrosion on USAF aircraft. *Material Evaluations* **52**(1), 64–73 (January 1994).
2. D. L. Balageas, J. C. Krapez and P. Cielo, Pulsed photothermal modelling of layered materials, *J. Appl. Physics* **59**(2), 348–357 (1986).
3. X. Maldague, *Nondestructive Evaluation of Materials by Infrared Thermography*. Springer, London (1992).
4. H. I. Syed and K. E. Cramer, Corrosion detection in aircraft skin, *Proc. SPIE* Vol 1933, *Thermosense*—XV, pp. 160–163 (1993).
5. N. K. DelGrande, K. W. Dolan, P. F. Durbin, M. R. Gorvad and A. B. Shapiro. Dynamic thermal tomography for nondestructive inspection of aging aircraft, *Proc. SPIE*, Vol 2001 NDI of aging aircraft (1993).
6. N. K. DelGrande, K. W. Dolan, P. F Durbin, M. R. Gorvad, B. T. Kornblum, D. E. Perkins, D. J. Schneberk and A. B. Shapiro. Three-dimensional dynamic thermal imaging of structural flaws by dual-band infrared computed tomography, *Proc. SPIE*, Vol. 1942 Underground and obscured object imaging and detection (1993).
7. J. C. Batsale, D. Maillet et A. Degiovanni. Extension de la méthode des quadripoles thermiques à l'aide de transformations intégrals—Calcul d'un transfert thermique au travers d'un dfaut plan bidimensionnel, *Int. J. Heat Mass Transfer* **37**(1), 111–127 (1994).
8. H. S. Carslaw and J. C. Jaeger, *Conduction of Heat in Solids*. Oxford University Press, Oxford (1978).
9. V. Vavilov, P. G. Bison, C. Bressan, E. Grinzato and S. Marinetti, Informative parameters and noise in transient thermal NDT. In *Advances in Signal Processing for Nondestructive Evaluation of Materials*. NATO ASI Series E: Applied Sciences, Vol. 262. Kluwer Academic (1994).
10. L. D. Favro, D. J. Crowther, P. K. Kuo and R. L. Thomas, Inversion of pulsed thermal-wave images for defect sizing and shape recovery, *Proc. SPIE*, Vol. 1933 *Thermosense*—XV, pp. 178–181 (1993).
11. E. R. G. Eckert and R. M. Drake, *Analysis of Heat and Mass Transfer*. McGraw-Hill, New York (1972).